

Detection of a new sample of Galactic White Dwarfs in the direction of the Small Magellanic Cloud

A.V. Sidharth^{1*}, B. Shridharan^{1,3}, Blesson Mathew¹, A. Devaraj¹, T.B. Cysil¹, C. S. Stalin², R. Arun², Suman Bhattacharyya¹, Sreeja S. Kartha¹, and T. Robin¹

¹ Department of Physics and Electronics, CHRIST (Deemed to be University), Bangalore 560029, India

² Indian Institute of Astrophysics, Sarjapur Road, Koramangala, Bangalore 560034, India

³ Tata Institute of Fundamental Research, Homi Bhabha Road, Mumbai 400005, India

Received xxxx; accepted xxxx

ABSTRACT

Aims. In this study, we demonstrate the efficacy of the Ultraviolet Imaging Telescope (UVIT) in identifying and characterizing white dwarfs (WDs) within the Milky Way Galaxy.

Methods. Leveraging the UVIT point source catalogue towards SMC and crossmatching with Gaia DR3 data, we identified 43 single WDs (37 new detections), 13 new WD+main sequence (MS) candidates and 161 UV bright MS stars by analysing their Spectral Energy Distributions (SED). Using the WD evolutionary models, we determine the masses, effective temperatures, and cooling ages of these identified WDs.

Results. Masses of these WDs range from 0.2 to 1.3 M_{\odot} and effective temperatures (T_{eff}) between 10000 K to 15000 K, with cooling ages spanning 0.1 to 2 Gyr. Notably, we detect hotter WDs compared to literature values, which is attributed to the sensitivity of UVIT. Furthermore, we report the detection of 20 new extremely low-mass (ELM) candidates from our analysis. Future spectroscopic studies of the ELM candidates will help us understand the formation scenarios of these exotic objects. Despite limitations in Gaia DR3 distance measurements for optically faint WDs, we provide a crude estimate of the WD space density within 1kpc as $1.3 \times 10^{-3} \text{ pc}^{-3}$, which is higher than previous estimates in the literature.

Conclusions. Our results underscore the instrumental capabilities of UVIT and anticipate the forthcoming UV missions like INSIST for systematic WD discovery. Our methodology sets a precedent for future analyses in other UVIT fields to find more WDs and perform spectroscopic studies to verify their candidacy.

Key words. (Stars:) white dwarfs – Ultraviolet: stars – Techniques: photometric – (stars:) Hertzsprung–Russell and colour–magnitude – (stars:) binaries: general

1. Introduction

White Dwarfs (WDs) are the end stages of stellar evolution for the majority of main-sequence (MS) stars with masses less than 8 M_{\odot} , which live out their life dissipating their remnant energy and cool down (Fontaine et al. 2001). The census and characterization of WDs have witnessed significant advancements, propelled by the utilization of various optical surveys such as Gaia Data Release 2 (DR2) (Gaia et al. 2018), Gaia Data Release 3 (DR3) (Brown et al. 2021), and Sloan Digital Sky Survey (SDSS) (York et al. 2000). Works of Gentile Fusillo et al. (2019, 2021), Kepler et al. (2016, 2019, 2021), and Eisenstein et al. (2006) have significantly refined our understanding of WDs. Accurate parallax measurements from Gaia DR2 and DR3 have revolutionized the study of WDs, enabling an unprecedented scale of search for these stellar remnants. Jiménez-Esteban et al. (2018) identified ~ 73,000 WD candidates, delving into a detailed exploration of the population within the 100 pc solar neighbourhood. Extending this effort, Gentile Fusillo et al. (2019) used Gaia DR2 to identify ~ 260,000 WD candidates, whereas Gentile Fusillo et al. (2021) presented a compilation of ~ 359,000 high-confidence WD candidates spanning all sky using Gaia EDR3.

On the other hand, hot WDs (with $T_{eff} \geq 10000$ K) remained elusive in these optical surveys as they have low optical luminosity and optical colours are insensitive to hotter temperatures (Gómez de Castro & Barstow 2007). The operation of the Galaxy Evolution Explorer (GALEX) ultraviolet sky survey (Morrissey et al. 2007), Bianchi et al. (2011), utilized GALEX to identify hot WDs in the Milky Way. UV point source catalogues stand as invaluable gateways into the studies of UV-bright MS stars, blue straggler stars (BSS), yellow straggler stars, sub-subgiants, WDs, and white dwarf – main sequence (WD+MS) binary systems (Bianchi 2009; Bianchi et al. 2011; Parsons et al. 2016; Rebassa-Mansergas et al. 2017; Subramaniam et al. 2018; Ren et al. 2020). The UV surveys, in combination with optical photometry, help us to characterize these systems and understand the end stages of stellar evolution. Rebassa-Mansergas et al. (2021) studied WD+MS systems using Gaia EDR3 to identify a volume-limited sample of 112 unresolved WD+MS binaries within 100 pc. Combining astrometric and photometric data from Gaia DR3 with GALEX GR6/7, Nayak et al. (2024) identified 93 WD+MS candidates. Recently, Jackim et al. (2024) presented the GALEX - Gaia EDR3 catalogue containing 332,111 candidate WD binary systems and 111,996 candidate single white dwarfs.

Ultra Violet Imaging Telescope (UVIT) onboard AstroSat mission is a suite of Far Ultra Violet (FUV: 130 - 180 nm),

* E-mail: sidharthnarayanan17@gmail.com

Near Ultra Violet (NUV: 200 - 300 nm) and Visible band (VIS: 320-550 nm) imagers. UVIT can perform simultaneous observations in these three channels with a field of view (FoV) diameter of $\sim 28'$ and an angular resolution of 1.5-1.8'' (more details on UVIT can be found in Kumar et al. 2012; Tandon et al. 2017a and Tandon et al. 2017b). The higher angular resolution of UVIT, compared to the 4.2-5.3'' angular resolution of GALEX (Morrissey et al. 2007), and the availability of seven filters in the UV range (1161 Å – 2882 Å) compared to two filters in GALEX, help us characterise WD systems with better precision compared to previous studies conducted using GALEX. Previous studies using UVIT observations have identified WDs and WD binary systems in open clusters and globular clusters, as evident from a series of UVIT Open Cluster studies (eg: Panthi & Vaidya 2024; Panthi et al. 2023; Vaidya et al. 2022; Sindhu et al. 2019; Jadhav et al. 2019) and Globular Cluster UVIT Legacy Survey (Glob-ULeS) studies (eg: Dattatreya et al. 2023a,b; Prabhu et al. 2022; Sahu et al. 2022), thus showcasing the superior capabilities of the UVIT instrument.

In this study, we use the UVIT point-source catalogue from Devaraj et al. (2023) to explore the FUV (1300 – 1800 Å) and NUV (2000 – 3000 Å) observations directed towards a previously less explored line of sight towards the Small Magellanic Cloud (SMC). As a follow-up to the UVIT point-source catalogue provided by Devaraj et al. (2023), we crossmatch them with the Gaia DR3 catalogue (Gaia Collaboration et al. 2023). This allows us to combine the photometric data from 7 UV filters and the optical photometry and astrometry from Gaia DR3 in order to identify and characterise the UV bright sources in the FoV of the SMC. The availability of 7 UV data points allows the generation of a better fit to the Spectral Energy Distributions (SED), providing more accurate parameters.

The manuscript is structured as follows. In Section 2, we describe the data used in this study and discuss the methodology employed for cross-matching the UVIT point-source catalogue with Gaia DR3. Section 3 presents the methodology for identifying MS, WD and WD+MS systems in our sample. Further, by combining UV photometry with available optical photometry, we fit the SED of each source to characterise the identified sources. We estimate the mass and cooling ages of our WD and WD+MS candidates and compare those parameters with values from the literature. Section 4 discusses the identification of Extremely Low-Mass WD (ELM) candidates in our sample. We also discuss the completeness of our WD identification and its implications on WD space density estimates. A summary of our findings is encapsulated in Section 5.

2. Data used in this study

We made use of the UVIT point-source catalogue (hereafter, SMC-UVIT-1), which includes the observations taken at three fields with combined FoV of $\sim 40'$ towards the SMC (centred at $\alpha_{2000} = \sim 17.285^\circ$ & $\delta_{2000} = \sim -71.329^\circ$), between 2017 December 31 and 2018 January 1 (Devaraj et al. 2023). The three fields were shifted $\sim 6'$ in an orthogonal direction from each other, with some level of overlap between them. The first field was chosen far away from the centre of the SMC to avoid the bright central region (Tandon et al. 2020). Figure 1 shows the grey-scale mosaic of the three SMC fields observed by UVIT in the N245M filter. UVIT has an impressive $\sim 1.5''$ spatial resolution which is better than the $\sim 5''$ spatial resolution of GALEX or $\sim 3''$ spatial resolution of Ultraviolet Imaging Telescope (UIT) (Stecher et al. 1997). For further details on the exposure time

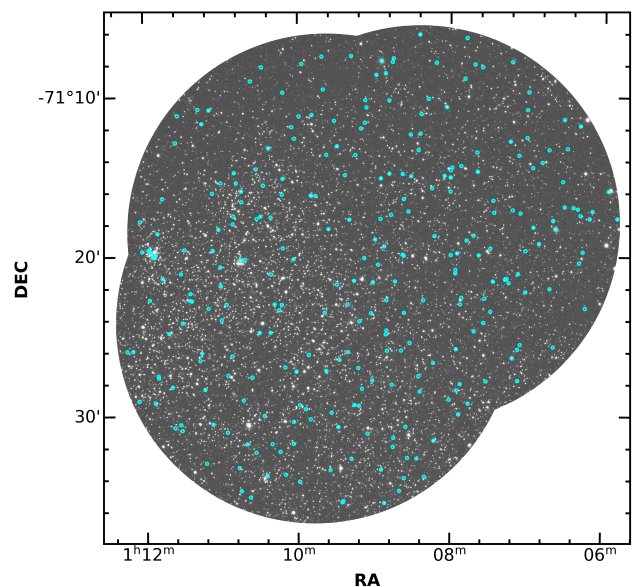


Fig. 1. The greyscale mosaic of the three SMC fields observed by UVIT in the N245M filter. The image was convolved by a Gaussian kernel of 1.5'' for better visualization. The sample of 273 sources in this study is given in cyan open circles.

and the information on different filters used, refer to Devaraj et al. (2023). SMC-UVIT-1 has a combined total of 11,241 objects detected across 7 UVIT filters viz *F154W*, *F169M*, *F172M*, *N245M*, *N263M*, *N279N* and *N219M*, with a limiting magnitude of ~ 21 mag.

We cross-matched the SMC-UVIT-1 and Gaia DR3 catalogue¹ to complement our UV data with astrometric and optical photometric information. The cross-matching was performed employing a search radius of 1.5'', aligning with the spatial resolution of the UVIT instrument. This resulted in a source list of 10,847 objects having both UVIT and Gaia measurements (hereafter SMC-UVIT-Gaia). The average offset in angular separation between the corresponding UVIT and Gaia sources is around 0.1'', with $\sim 90\%$ of the sources matching within 0.4''.

We applied the following astrometric and photometric quality criteria to the Gaia DR3 catalogue, adapted from Rebassa-Mansergas et al. (2021):

- $I_{BP}/\sigma_{I_{BP}} \geq 10$
- $I_{RP}/\sigma_{I_{RP}} \geq 10$
- $I_G/\sigma_{I_G} \geq 10$
- $\varpi/\sigma_\varpi \geq 3$
- $\varpi > 0$

where ϖ is the parallax in arcseconds, I_G , I_{BP} and I_{RP} are the fluxes in the bandpass filters *G*, *G_{BP}* and *G_{RP}*, respectively, and the σ values are the standard errors of the corresponding parameters. Further, we applied the following photometric quality criteria to the available UVIT magnitudes:

- $M_X/\sigma_{M_X} \geq 10$

where M_X and σ_{M_X} represent the magnitude and the error in magnitude in each of the seven UVIT filters. It is to be noted that not all stars have UVIT magnitudes in all 7 filters.

From the sample of 10,847 sources, 273 sources qualified the given criteria, with 87.9% of the sources having Renormalised

¹ <https://gea.esac.esa.int/archive/>

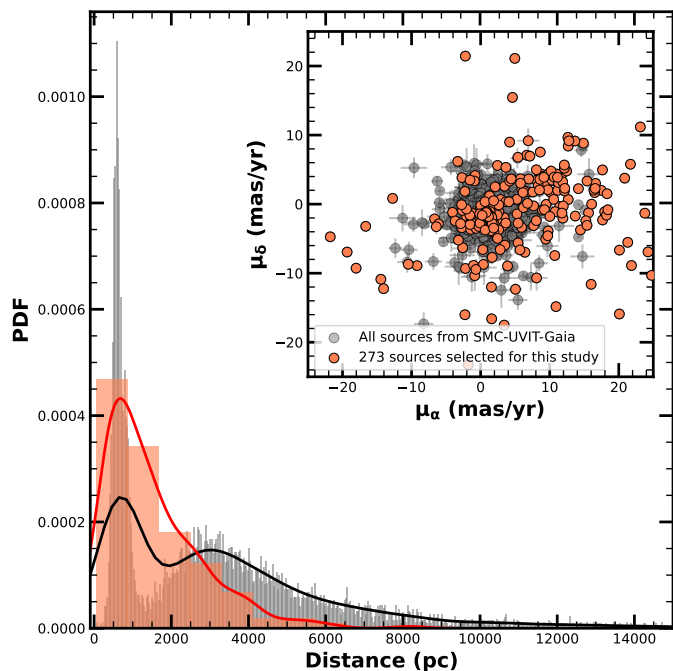


Fig. 2. Gaia DR3 distance (Bailer-Jones et al. 2021) distribution plot of the 273 sources used in this study. The 273 sources used in this study are given in orange and the 10,847 sources in the SMC-UVIT-Gaia in grey markers. Kernel density estimates (KDE) of the distributions are overlaid for a better visual representation. The red and black lines are the KDE plots of the 273 sources and SMC-UVIT-Gaia sources, respectively. In the inset: Scatter plot with error bars of proper motion in RA (mas/yr) vs proper motion in Dec (mas/yr). For most sources, error bars are of the size of the markers.

Unit Weight Error (RUWE) ≤ 1.4 . About 76% of 273 sources have data in at least 3 UV filters in addition to the 3 Gaia optical filters. This dataset comprising 273 sources having robust photometric and astrometric information is used in this study.

3. Analysis and Results

3.1. Do the sources belong to SMC or the Milky Way?

A critical aspect of our analysis is to discern whether our sample of 273 sources belong to SMC or if they are Milky Way (MW) sources projected in the line of sight to the SMC. To accomplish this, we leveraged the distance data provided by Gaia DR3 for all the sources (Bailer-Jones et al. 2021), which is depicted as a histogram in Figure 2. Our 273 sources lie within the distance range of 50 pc – 6500 pc, with the maximum distance recorded at 8176 ± 769 pc. Notably, the SMC is situated at a distance of 61.9 ± 0.6 kpc (De Grijs & Bono 2015), establishing a stark contrast between our sources’ distances and the known distance of SMC. In addition to the distance values, from the plot of proper motion in Dec (μ_δ) vs proper motion in RA (μ_α) given in Figure 2 (inset), it is clear that the majority of 273 sources have higher values compared to the rest of the SMC-UVIT-Gaia sources. This confirms that the 273 sources belong to the MW, and is found to be in the projection of the SMC.

Furthermore, to have an understanding of the types of sources in our sample, we performed a SIMBAD crossmatch of the 273 sources and found that 24 sources have previous classifications in the literature. We note that six sources are classified as WD candidates (WD*_candidate) by Gentile Fusillo et al. (2021). Out of these six WD candidates, Gaia DR2

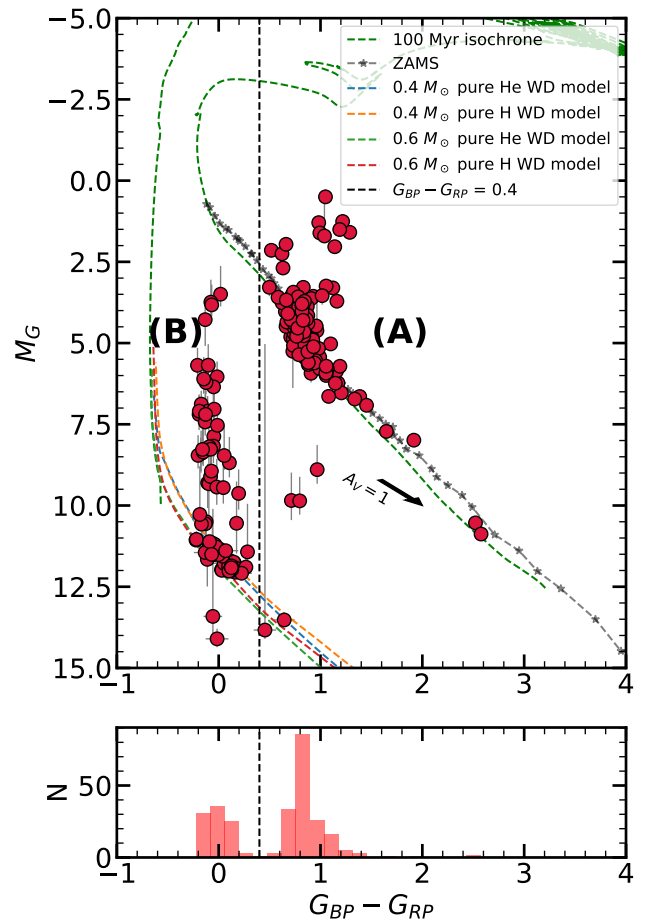


Fig. 3. Top panel: Extinction corrected Gaia CMD of the 273 sources (red-filled circles) with $G_{BP} - G_{RP}$ on the X-axis and M_G on the Y-axis. The black vertical line that divides the CMD into two populations is $G_{BP} - G_{RP} = 0.4$. The black arrow shows the reddening vector for $A_V = 1$ mag. Bottom panel: The number distribution of the 273 sources in the $G_{BP} - G_{RP}$ colour.

4690619477160130944 was also listed as a WD candidate in Jiménez-Esteban et al. (2018). 13 are classified as ‘star’. Two sources are classified as ‘RGB*_candidate’, one as RR Lyrae Variable (RRLyra), one as a high proper motion star (PM^*) and one as a Classical Cepheid Variable (δCep). We also cross-matched our list of 273 sources with the WD catalogue provided by Jackim et al. (2024) and found 12 matches. One of the sources classified as a WD candidate by Jackim et al. (2024) was also classified as a WD candidate by Gentile Fusillo et al. (2021). The list of these objects is given in Table A.1.

3.2. Disentangling MS Sources and WD Sources

As seen with the literature crossmatch, we expect to find MS, RGB and WD sources in our sample. With the exceptional astrometry from Gaia, we create a Gaia Color-Magnitude Diagram (CMD) and segregate the sample of MS/RGB and WD sources based on their positions in the CMD.

We plot the absolute G band magnitude M_G against $G_{BP} - G_{RP}$ color for 273 sources in Figure 3 along with the Zero Age Main Sequence (ZAMS) (Pecaut & Mamajek 2013), a 100 Myr isochrone from Modules for Experiments in Stellar Astrophysics

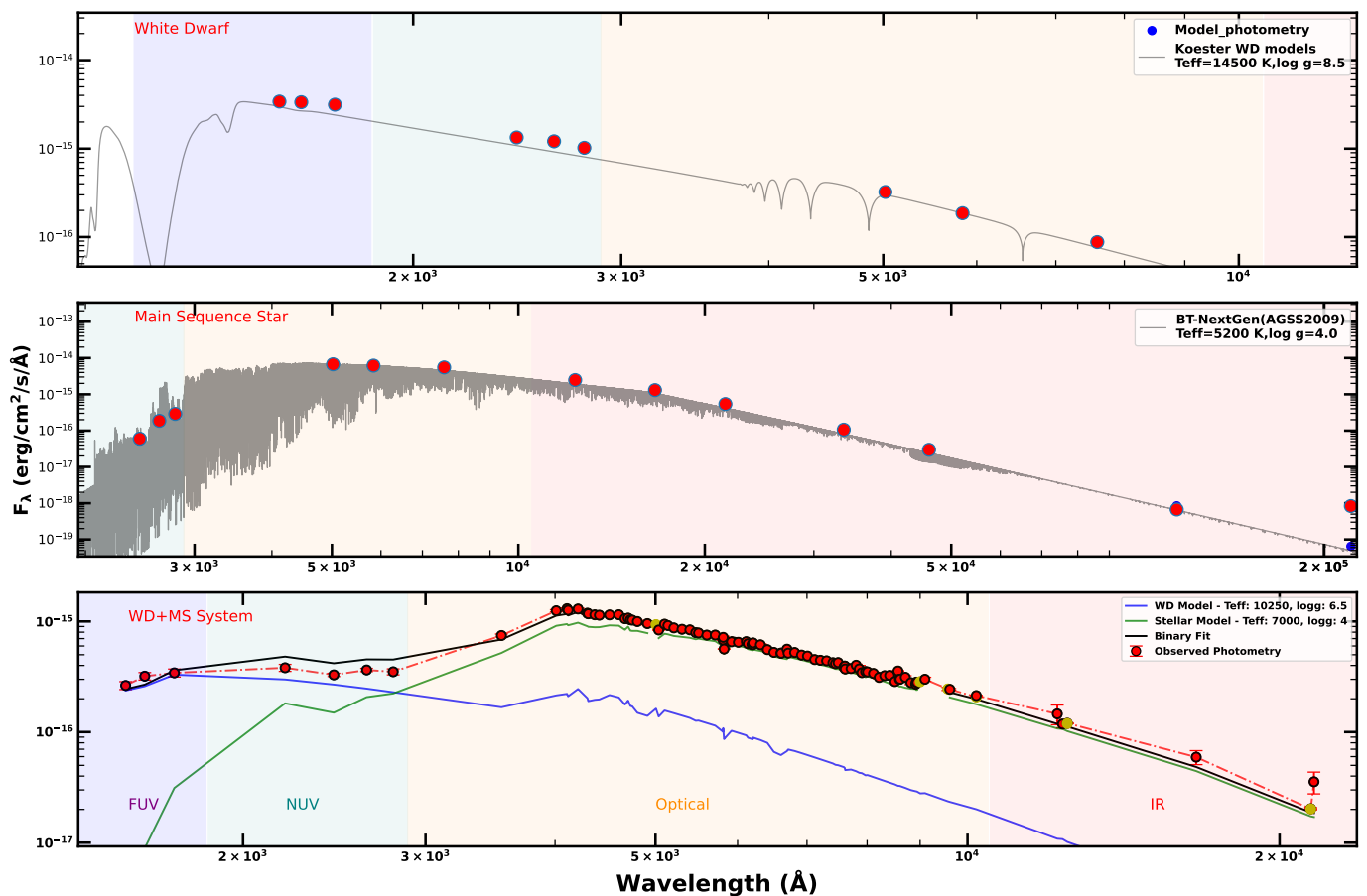


Fig. 4. A representative sample of SEDs of WD (Gaia DR3 4690625700572457088), MS star (Gaia DR3 4690614052626726016), WD+MS (Gaia DR3 4690657483318685312) over-plotted by their respective best-fitted models. The scaling of the X-axis and Y-axis of each plot are different.

(MESA)² (Choi et al. 2016; Dotter 2016) and WD cooling tracks from Bédard et al. (2020). The CMD shows a diverse population including WDs, MS stars, and potential WD+MS star systems. A clear distinction can be seen in the CMD and we use $G_{BP} - G_{RP} > 0.4$ mag as the cutoff to separate MS and WD sources (shown as regions A and B, respectively). The bottom panel in Figure 3 shows a clear distinction between the population at $G_{BP} - G_{RP} = 0.4$. This distinction aligns with the expected optical brightness contrast between MS stars and WDs, enabling a reliable differentiation. This approach is based on the fact that WDs will be brighter in bluer bands and MS stars in redder. WDs emit a significant amount of their radiation in the blue and ultraviolet parts of the spectrum. As a result, they tend to be brighter in bluer bands (in this case, BP mag) compared to MS stars. The cutoff yielded 95 potential WD sources in region B, and 178 potential MS stars in region A, exhibiting characteristics consistent with MS stars. The SMC is characterized by a notably low foreground extinction value of $E(B-V) = 0.02$ mag (Hutchings 1982), representing the maximum potential extinction that our sources could encounter in this line of sight. Hence, for the purposes of our analysis, we are considering an extinction value of $A_V = 0.062$ mag, which corresponds to $E(B-V) = 0.02$ mag for the sources.

3.3. SED analysis of UV-Bright MS and WD sources

To characterise the 178 potential MS sources, we employed a Python-based routine tailored to fit observed SEDs, similar to the SED routine used in Arun et al. (2021), Bhattacharyya et al. (2022) and Shridharan et al. (2022). The SED for a target object is constructed using photometric data from various sources spanning wavelengths from far-UV to far-IR, including available photometry from *UVIT*, *UCAC4*, *SDSS*, *Gaia*, *2MASS*, *AKARI IRC*, *AKARI FIS*, *WISE*, and *IRAS*. SED templates used for the fitting process are derived from the BT-NextGen (AGSS2009) model grid (Allard et al. 2011, 2012), considering the parameters of effective temperature ($800\text{K} \leq T_{\text{eff}} \leq 70000\text{K}$), surface gravity ($-0.5 \leq \log g \leq 6$) and metallicity ($-4 \leq [Fe/H] \leq 0.5$).

The fitting procedure involved a normalization process of observed and model photometry, utilizing user-specified bands. The determination of the best-fit model relied on minimizing the chi-squared parameter (χ^2), computed from fitting the *UVIT* bands, *Gaia* *G*, G_{BP} , and G_{RP} band photometry, thereby giving the most suitable model corresponding to the lowest χ^2 . Subsequently, stellar parameters such as T_{eff} and $\log g$ are estimated from the SED fitting. Upon visual inspection of fit quality, our analysis revealed that 161 sources out of 178, exhibited very good fit with theoretical models, indicative of their classification as UV-bright MS stars (provided in Table B.1). Out of 161 sources, $\sim 89\%$ of the sources have $\log g$ ranging from 4 to 5.5. The T_{eff} of these sources range from 4500 K to 6500 K. Conversely, 16 stars encountered fitting discrepancies that can be pri-

² <https://waps.cfa.harvard.edu/MIST/>

marily attributed to problematic photometric data or the presence of a companion and will be further analysed in Section 3.4.

To characterize the WD sources, we fit the Koester WD models for pure H atmospheres (Koester 2010) to the 95 sources lying in region B of the Gaia CMD. The fitting process involves a systematic comparison between observed SEDs and theoretical WD models. By assessing various parameters, such as T_{eff} and $logg$, the routine determines the most suitable WD model that best matches the observed data. Subsequently, the fitted SEDs underwent a visual classification, categorizing them based on the goodness of their fit. 43 of 95 sources showed a very good SED fit, indicating them being highly probable WD candidates. Checking against the existing literature, 37 out of these 43 WDs are found to be new detections. Four sources (Gaia DR3 4690615216552295808, Gaia DR3 4690615560150914560, Gaia DR3 4690613017528995840, Gaia DR3 4690659300093357184) were previously classified as highly probable WD candidates by Gentile Fusillo et al. (2021) and two sources (Gaia DR3 4690616659661394304, Gaia DR3 4690551758417486336) were classified as WD candidates in Jackim et al. (2024). These are marked by boldface in Table 1. Furthermore, the stellar parameters encompassing critical factors such as effective temperature and surface gravity for the identified 43 WDs are tabulated in Table 1. The SED analysis resulted in 52 sources which couldn't be fitted with a single WD model. Some of these sources showed optical or IR excess. These objects will be looked into in detail in the next section as potential WD+MS sources.

3.4. Identifying WD+MS Binaries

WD+MS binaries pose a unique challenge since the flux of one of the stars dominates the SED, making their identification in the HR diagram elusive. These systems will have similar magnitudes and colours as single stars. However, systems where both the WD and MS companion contribute significantly to the optical flux, form a bridge between the WD and MS loci in the CMD (Rebassa-Mansergas et al. 2021). Our initial analysis revealed that our sample may also include WD+MS binary systems since some objects lie between the WD locus denoted by the WD cooling tracks and MS loci indicated by the ZAMS in Figure 3 displaying the CMD.

Our strategy involved visually classifying SEDs showing optical and IR excess during WD model fitting or the sources that were not fitting well with the single WD model as potential binary systems. This resulted in the identification of 52 such sources. Utilizing the VO SED analyzing tool (VOSA³; Bayo et al. 2008), we fitted binary models for these candidates. For the MS star component in our binary modelling, we utilized the BT-Settl-CIFIST models (Baraffe et al. 2015), offering a wide database of spectra across T_{eff} ranging from 1,200 K to 7,000 K, with $logg$ within $4 \leq logg \leq 5$. For H-rich WDs, we employed Koester (2010) WD evolution models (Koester 2010), with T_{eff} between 5,000 K and 80,000 K, and $logg$ within $6.5 \leq logg \leq 9.5$.

Among these 52 sources, visual inspection revealed 13 stars exhibiting good fit, implying them being potential binary systems. A representative sample of a well-fitted WD+MS system is shown in the bottom panel of Figure 4. Table 2 presents the parameters of these selected WD+MS binary candidates. Notably, we refrained from relying on reduced chi-square parameters provided by VOSA. Existing literature (Rebassa-Mansergas et al.

2021; Nayak et al. 2024) has cautioned against their use due to potentially misleading outcomes. Instead, we used the prevalent and accepted parameter called visual goodness-of-fit ($Vgfb$) provided by VOSA along with visually inspecting the goodness of fit in our analysis. All 13 candidates have $Vgfb < 15$, which is usually considered as a proxy for well-fitted SEDs.

3.5. Estimation of Mass and the cooling age of WDs and WD+MS candidates

The determination of WD masses is crucial in understanding their physical properties and evolution. While the mass can be derived during SED fitting, its accuracy heavily depends on the derived $logg$ of the WD. However, since SED is essentially a low-resolution spectrum, the $logg$ derived from SED fitting may not be precise, leading to unreliable mass estimates.

To overcome this limitation, we adopt a method commonly used in the literature (e.g., Nayak et al. 2024; Karinkuzhi et al. 2024), which utilizes the model cooling curves of WDs to estimate their masses. For this purpose, we utilize the 'WD_models' Python open-source package⁴, which facilitates the conversion between WD optical photometry and physical parameters (Cheng et al. 2020). Specifically, we employ the cooling models developed by Bédard et al. (2020)⁵, which account for WDs with thick H atmospheres and CO cores. 'WD_models' estimates the mass and other parameters by finding the closest atmosphere grid and cooling model in the Gaia CMD.

By applying this methodology, we try to estimate the masses of 43 single WDs using their Gaia photometry. Among these WDs, 19 falls within the mass range covered by the available models, which spans from $0.2 M_{\odot}$ to $1.3 M_{\odot}$. Consequently, we estimate the masses for these 18 WDs. However, the remaining 24 WDs have masses below $0.2 M_{\odot}$ and exhibit luminosities exceeding the model evolutionary tracks. As a result, we cannot estimate the masses for these sources through this method. Furthermore, we estimate the mass of the WD component of the 13 WD+MS candidates identified in this paper using the same method. We find that 12 of 13 sources lie within the model range and we estimate the masses for them. One WD+MS candidate has a mass below $0.2 M_{\odot}$ and its mass cannot be calculated for the same reason mentioned earlier. Masses of the WD components range between $0.3 M_{\odot}$ to $0.6 M_{\odot}$.

In addition to the WD masses, we can also estimate the cooling age of these WDs from the model tracks using the 'WD_models' package. The cooling age of the single WDs ranges from 0.1 Gyr to 1.9 Gyr whereas for the WD components of the WD+MS binaries, cooling ages range from 0.2 Gyr to 0.6 Gyr. The mass and cooling age of single WDs and the WD+MS components are given in Table 1 and Table 2, respectively.

3.6. Comparison with existing WD and WD+MS catalogues

It is important to compare the derived values of our sample to the values present in the literature on WDs. We made use of the Montreal White Dwarf Database⁶ (Dufour et al. 2016), a collection of confirmed white dwarfs in the literature. We selected single DA white dwarfs with at least one spectra available as our bonafide sample of WDs. We also removed WDs which show

⁴ https://github.com/SihaoCheng/Wd_models

⁵ Available at <http://www.astro.umontreal.ca/~bergeron/CoolingModels/>

⁶ <https://www.montrealwhitedwarfdatabase.org/home.html>

³ <http://svo2.cab.inta-csic.es/theory/vosa/>

Table 1. List of the 43 single white dwarfs identified in the present study. The WDs marked in bold were previously detected in the literature as WD candidates.

RA (deg)	DE (deg)	Distance (pc)	N263M (mag)		N245M (mag)		N279N (mag)		F172M (mag)		F169M (mag)		F154W (mag)		N219M (mag)		T _{eff} (K)	logg	Cooling Age (Gyr)	WD Mass (M _⊙)
			AB	Error																
17.69418	-71.55454	542 ⁺⁴⁷ ₋₁₁	19.779	0.051	19.895	0.047	19.598	0.088	19.876	0.082	20.168	0.078	19.929	0.066			12500	6.75	0.1	0.35
17.66857	-71.52984	258 ⁺¹¹ ₋₃₀₃	18.644	0.03	18.679	0.027	18.8	0.061	18.801	0.057	18.761	0.041	18.944	0.042	18.619	0.055	13250	8.5		ELM
17.80608^α	-71.47253	1173 ⁺³¹⁹ ₋₅₃₈	18.959	0.035	18.944	0.03	19.067	0.069	19.078	0.057	19	0.046	19.099	0.045	18.957	0.064	13250	8.25		ELM
17.22698	-71.55645	1008 ⁺²¹⁹ ₋₁₄₈	19.01	0.036	19.171	0.034	19.056	0.069	19.158	0.059	19.399	0.055	19.575	0.056			11250	6.75		ELM
17.14111	-71.54422	492 ⁺³⁶ ₋₄₅			21.548	0.101			21.334	0.161			21.786	0.155			11250	6.75	0.54	0.51
17.38993	-71.49697	514 ⁺¹⁷⁸ ₋₄₃	20.409	0.049	20.579	0.046	20.53	0.098	20.463	0.077	20.733	0.07	20.846	0.072	20.496	0.129	11000	6.5	0.24	0.42
17.51403	-71.50647	1427 ⁺¹⁴⁰⁷ ₋₄₇₇	19.687	0.036	19.724	0.031	19.652	0.064	19.745	0.077	19.787	0.066	20.065	0.07	19.783	0.093	11750	6.75		ELM
17.58956	-71.41328	448 ⁺³⁶ ₋₂₈	20.018	0.033	20.129	0.031	20.227	0.069	20.03	0.062	20.435	0.064	20.279	0.055	20.202	0.084	12000	6.5	0.29	0.43
17.28988	-71.47199	435 ⁺²¹ ₋₁₆			21.758	0.08							22.164	0.183	21.344	0.176	10250	6.5	0.45	0.4
17.33562	-71.43358	461 ⁺³⁹ ₋₂₉	20.463	0.042	20.472	0.036	20.523	0.104	20.732	0.082	20.698	0.056	20.982	0.066	20.366	0.082	12750	8.5	0.35	0.47
17.05608	-71.44488	450 ⁺¹⁷ ₋₃₀	20.155	0.035	20.294	0.033	20.085	0.064	20.651	0.072	20.696	0.056	20.963	0.064	20.252	0.081	11250	7.25	0.26	0.41
17.57628	-71.3837	863 ⁺⁷⁶⁵ ₋₄₇₇	19.375	0.025	19.443	0.022	19.307	0.044	19.688	0.043	19.743	0.035	19.896	0.038	19.349	0.052	11500	7.5		ELM
17.51368	-71.33661	4663 ⁺¹¹⁴⁶ ₋₁₇₃₇	18.087	0.013	18.177	0.013	18.182	0.026	18.336	0.023	18.488	0.02	18.54	0.02	18.175	0.025	12750	8.25		
16.7787	-71.46324	398 ⁺⁶⁶ ₋₂₇	20.857	0.083	20.669	0.067	20.808	0.15	21.097	0.103	21.182	0.086	21.493	0.102			11000	6.75	0.51	0.56
16.77949	-71.4307	480 ⁺³² ₋₂₂	20.854	0.083	20.949	0.076	20.59	0.136	21.036	0.137	21.286	0.093	21.496	0.099			11000	6.75	0.34	0.55
16.56812	-71.32855	502 ⁺³⁶ ₋₂₅	20.567	0.073	20.764	0.07	20.557	0.134	20.761	0.121	21.022	0.105	20.943	0.105			12000	7.5	0.33	0.57
16.71119^α	-71.31982	1554 ⁺³³⁶ ₋₇₂₄	18.639	0.03	18.767	0.028	18.618	0.055	18.784	0.049	18.867	0.039	19.071	0.044	18.782	0.053	12000	7.25		ELM
16.98139	-71.43035	5410 ⁺¹⁷²⁴ ₋₁₅₈₅	18.026	0.013	18.08	0.012	18.007	0.024	18.217	0.022	18.235	0.018	18.313	0.018	18.058	0.028	12250	7.75		
16.86897	-71.39106	498 ⁺⁷⁸ ₋₂₄	21.671	0.087	21.585	0.074	21.358	0.194	21.672	0.135	21.909	0.103	21.892	0.106			10750	6.5	0.55	0.54
17.15645^α	-71.33187	1860 ⁺⁵²⁶ ₋₄₁₆	18.827	0.019	18.855	0.017	18.877	0.036	18.869	0.03	18.884	0.024	18.931	0.024	18.773	0.032	14250	9		ELM
17.15341	-71.33289	557 ⁺²⁰ ₋₁₂	20.5	0.042	20.709	0.04	20.435	0.078	20.732	0.074	20.822	0.06	20.957	0.063	20.335	0.066	12500	8.5	0.14	0.59
17.31568^α	-71.35908	1889 ⁺²⁰⁸ ₋₂₃₂	18.928	0.02	19.056	0.019	19.084	0.04	19.128	0.034	19.228	0.028	19.274	0.028	18.976	0.035	12500	8		ELM
17.24697^β	-71.31595	1119 ⁺²²⁰ ₋₂₇₃	18.691	0.018	18.8	0.016	18.748	0.034	18.814	0.029	18.888	0.024	18.978	0.024	18.763	0.032	13500	8.5		ELM
16.90776	-71.33224	2377 ⁺⁸²⁴ ₋₈₂₄	18.897	0.02	18.995	0.018	18.939	0.038	19.099	0.033	19.127	0.027	19.238	0.028	19.051	0.046	11750	6.5		ELM
17.13819	-71.2866	524 ⁺⁶⁸ ₋₂₅	20.821	0.05	20.806	0.042	20.857	0.112	20.601	0.076	21.068	0.078	21.227	0.072	20.666	0.128	11500	7.25	0.31	0.57
17.12949	-71.24981	1534 ⁺⁵⁷⁵ ₋₄₄₃	19.256	0.023	19.293	0.021	19.249	0.044	19.463	0.039	19.492	0.031	19.601	0.033	19.332	0.049	12250	7.75		ELM
17.45362	-71.18575	470 ⁺²⁰⁵ ₋₂₀₅	20.415	0.049	20.543	0.045	20.503	0.096	20.743	0.086	21	0.082	21.085	0.088	20.487	0.084	11750	7.75	0.31	0.64
16.62831	-71.28139	1379 ⁺⁶⁵⁷ ₋₄₃₀	19.584	0.046	19.669	0.042	19.529	0.083	20.028	0.086	20.165	0.071	20.175	0.073	19.921	0.089	11250	6.75		ELM
16.48553	-71.26473	2612 ⁺⁴⁵⁹ ₋₄₅₉	17.784	0.02	17.834	0.018	17.84	0.038	17.675	0.029	17.748	0.023	17.823	0.025			15000	9		
17.09648	-71.18481	189 ⁺²⁷ ₋₁₅	21.591	0.118	21.602	0.073	21.198	0.18	21.456	0.167	21.804	0.155	22.258	0.192	21.056	0.154	11750	8.25	1.91	1.26
17.81519	-71.43458	631 ⁺³⁸ ₋₁₅	20.001	0.041	20.018	0.036	19.745	0.066	20.129	0.065	20.095	0.053	20.159	0.052	19.824	0.095	13000	8.5	0.09	0.29
17.84723	-71.38002	1478 ⁺³⁵⁵ ₋₂₆₅	19.663	0.034	19.803	0.032	19.497	0.059	20.064	0.068	19.913	0.047	20.073	0.05	19.552	0.057	14000	9.5		ELM
17.85196	-71.37223	1075 ⁺³⁷⁰ ₋₃₀₀	20.142	0.043	20.252	0.039	20.559	0.109	20.409	0.075	20.27	0.056	20.367	0.057	20.153	0.075	12500	7.75		ELM
18.00839	-71.32826	337 ⁺³⁰ ₋₃₀	20.173	0.045	20.221	0.039	20.128	0.079									12000	7.75	0.57	0.65
17.96764	-71.33433	2231 ⁺¹⁸⁵ ₋₁₈₅	18.749	0.023	18.821	0.02	18.667	0.04	18.952	0.053	19.041	0.043	19.132	0.045			11000	6.5		ELM
17.9879^α	-71.32667	1729 ⁺⁸⁹ ₋₃₈₁	19.066	0.026	19.249	0.025	19.092	0.051									11500	8.5		ELM
17.98428	-71.32692	1785 ⁺³⁸¹ ₋₃₈₀	19.307	0.03			19.156	0.07									11000	6.5		ELM
17.97703	-71.33103	874 ⁺²⁵⁴ ₋₃₁₂	19.334	0.042	19.426	0.027	19.245	0.073	19.284	0.062	19.391	0.051	19.366	0.051			14250	6.5		ELM
17.95815	-71.30935	882 ⁺⁴²⁴ ₋₁₄₉	19.415	0.03	19.617	0.029	19.651	0.066	19.778	0.077	19.93	0.065	19.98	0.067			11500	7		ELM
17.75881	-71.3053	3081 ⁺¹⁹⁸ ₋₁₈₈	18.608	0.021	18.591	0.019	18.679	0.041	18.773	0.035	18.713	0.027	18.761	0.027	18.503	0.035	13500	8.75		
17.63595	-71.24246	500 ⁺³⁷ ₋₆₇	20.761	0.047	20.902	0.045	20.611	0.082	21.067	0.084	21.363	0.078	21.465	0.088	20.613	0.125	12250	8.75	0.39	0.46
17.54867	-71.16241	422 ⁺³⁵ ₋₂₆	21.12	0.068	21.095	0.058	20.9	0.115	21.382	0.162	21.328	0.124	21.599	0.142			10750	6.5	0.52	0.44
17.40706 ^γ	-71.45349	269 ⁺¹⁸ ₋₂₆	18.76	0.019	18.91	0.017	18.757	0.034	19.112	0.033	19.132	0.027	19.245	0.028	18.887	0.043	11500	7.25	0.24	0.49

^α Gentile Fusillo et al. (2021), ^β Jackim et al. (2024), ^γ WD showing IR excess

Table 2. List of the 13 WD+MS candidates identified from the present study with the parameters of both the MS and WD components

RA (deg)	DE (deg)	Distance (pc)	N263M (mag)		N245M (mag)		N279N (mag)		F172M (mag)		F169M (mag)		F154W (mag)		N219M (mag)		MS_T _{eff} (K)	MS_logg	WD_T _{eff} (K)	WD_logg	WD Cooling Age (Gyr)	WD Mass (M _⊙)
			AB	Error																		
17.58841	-71.29290	430 ⁺²⁷ ₋₂₇	21.227	0.059	21.372	0.054			21.581	0.129	21.919	0.117	21.904	0.117	20.976	0.105	7000	4.5	13750	9.5	0.50	0.46

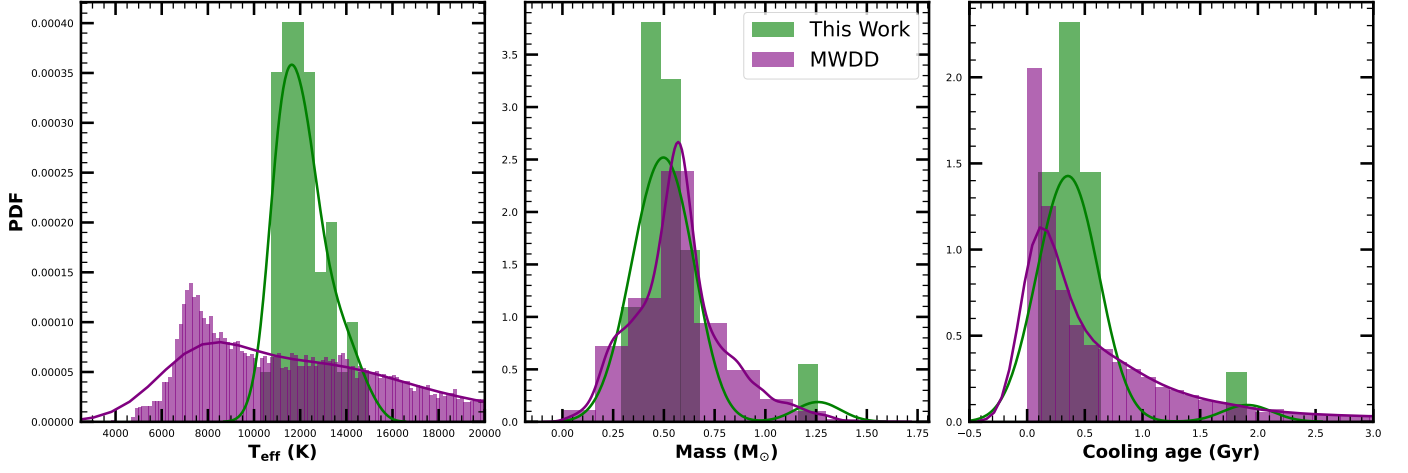


Fig. 5. Comparison of T_{eff} (K), mass (M_{\odot}) and the cooling age (Gyr) for single WDs identified in this work (green) and MWDD (purple). KDEs of the distributions are also overlaid for a better visual representation.

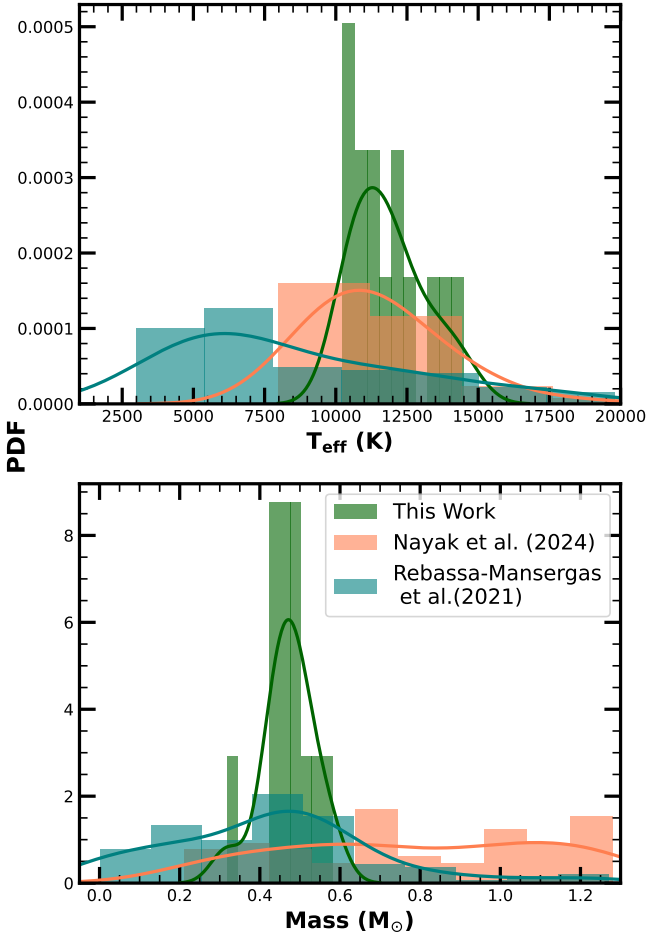


Fig. 6. Comparison of T_{eff} (K) and mass (M_{\odot}) of the WD component of the WD+MS candidates identified in this work with the works of Rebassa-Mansergas et al. (2021) and Nayak et al. (2024).

found by Nayak et al. (2024). We are identifying hotter WDs than both the previous studies.

4. Discussion

In this section, we discuss the population of WDs that do not fall under the WD locus and present the potential identification of a sample of ELMs in our sample. Furthermore, with the identified sample of WDs, we calculate the WD space density and compare it with the previous estimates.

4.1. Extremely-Low Mass White Dwarf Candidates

ELMs represent an exotic subset of WDs with masses below $0.3 M_{\odot}$, challenging the conventional understanding of single stellar evolution. These objects are expected to form via binary mass transfer from the WD progenitor during its red giant branch phase either through Roche lobe overflow or common envelope evolution (Istrate et al. 2014a,b; Nandez et al. 2015; Li et al. 2019; Pelisoli & Vos 2019; Brown et al. 2022; Nayak et al. 2024; Khurana et al. 2023). Kilic et al. (2007) established a minimal mass threshold of $\sim 0.3 M_{\odot}$ for WDs formed through standard evolutionary channels, considering the age of the Universe and associated timescales. Objects falling below this threshold necessitate alternative formation mechanisms, often linked to binary or multiple stellar systems. The mass and radius of a WD are inversely related (Parsons et al. 2017; Bédard et al. 2017). This implies that the ELMs exhibit larger radii, making them brighter than their canonical counterparts. Consequently, they occupy an intermediate region in the CMD, positioned between the MS locus and the locus of Single WDs.

Pelisoli & Vos (2019) defined a specific region in the Gaia CMD to identify the locus where ELMs are expected to appear. This region is defined by the equations:

$$M_G < 5.25 + 6.94 (G_{BP} - G_{RP} + 0.61)^{1/2.32} \quad (1)$$

$$M_G > 1.15 (G_{BP} - G_{RP}) + 6.00 \quad (2)$$

$$M_G > -42.2 (G_{BP} - G_{RP})^2 + 83.8(G_{BP} - G_{RP}) - 20.1 \quad (3)$$

where M_G is the absolute G magnitude calculated using Gaia G band magnitude.

As mentioned in Section 3.5, masses of 25 WDs (24 Single WDs and 1 WD+MS candidate) couldn't be found due to

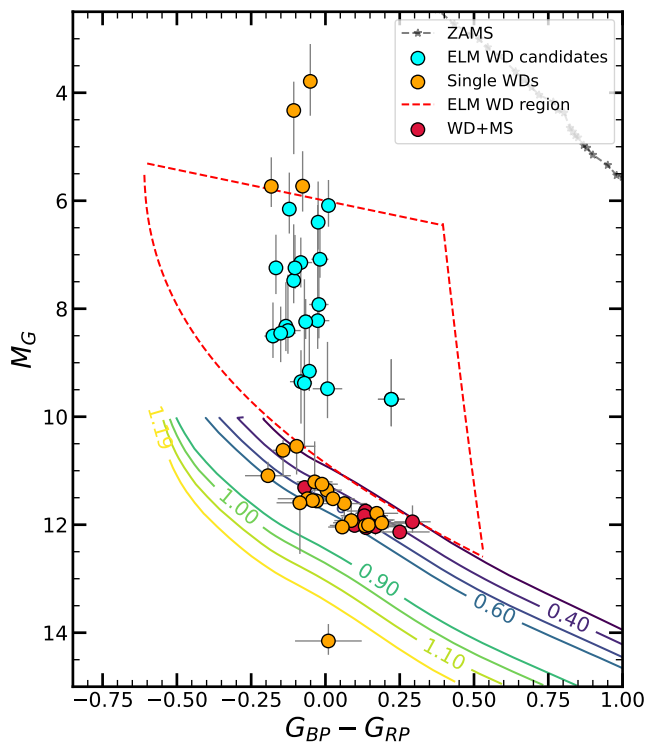


Fig. 7. Extinction corrected Gaia CMD of single WDs and WD+MS candidates from our classification. The ELM region is marked with red dotted lines. ELM WD candidates are shown with cyan-filled circles. The remaining single WDs and WD+MS candidates are shown with orange and red-filled circles, respectively. The WD cooling models for different masses from Bédard et al. (2020) are also overlaid. The numbers on the cooling track denote their corresponding masses in M_{\odot} .

their higher luminosity. In Figure 7, we plotted the above-defined ELM region on the Gaia CMD. 20 of these 25 high luminosity WDs fall within the defined ELM region. These 20 WDs serve as strong candidates for ELMs and are marked by ‘ELM’ in the ‘WD Mass’ column of Tables 1 and 2. They need to be followed up by spectroscopic observations to verify their candidacy. Follow-up studies of these 20 candidates will also allow us to constrain their physical parameters. The median distance of canonical mass WD sources from this study is ~ 500 pc, whereas, for ELM candidates, the median distance is ~ 1500 pc. We observe a higher percentage of ELMs in this study because ELMs are brighter than canonical mass WDs, resulting in better Gaia quality compared to WDs at a similar distance. Except for the extreme mass loss observed in high-metallicity stars (Kilic et al. 2007), ELM WDs are anticipated to originate from binary evolution, involving one or more instances of common envelope evolution (Li et al. 2019). Therefore, investigating ELM systems can provide valuable insights into the wider realm of binary interactions.

4.2. Completeness of WD detection

UV missions such as GALEX and UV-Excess survey (UVEX; Groot et al. 2009) have been instrumental in studying the hot DA white dwarf population within 1kpc of the Sun. Based on the photometrically identified DA population with $T_{eff} > 10,000$ K, the estimate of WD stellar density is $\sim 2.9-3.8 \times 10^{-4} \text{ pc}^{-3}$ within 1kpc (Verbeek et al. 2013). Hence, considering a cone of radius

$40'$ (FoV) at a distance of 1kpc, we can expect 48 DA WDs hotter than 10,000K. Using UVIT, we find 22 WDs hotter than 10,000K within 1kpc, providing a crude completeness estimate of 46% percentage.

However, it should also be noted that we are only considering the stars with good quality Gaia astrometry and photometry. As seen in Figure 2, there is a large population of sources with distances less than 2kpc that did not satisfy our quality criteria. This population might have many new WDs with low-quality Gaia astrometry and photometry. Upon relaxing the ϖ/σ_{ϖ} cut-off from ≥ 3 to ≥ 1 , we additionally find 552 WD candidates showcasing an exceptional fit to WD models in the SED analysis. Distance estimates provided by Gaia DR3 would not be accurate for these distant low-luminosity sources. Based on the SED fit, we see that these 552 sources have T_{eff} in the range of 7250K to 30,000K. Considering the UVIT sensitivity and degeneracies in mass, radius and $logg$, we estimate that they can be detected only to a distance limit of 8-10 kpc based on flux values of Koester (2010) model of a 30,000K WD. Assuming 8 kpc as the maximum distance of 552 WD candidates, we can estimate an upper limit to the WD stellar density as $\sim 5-6 \times 10^{-4} \text{ pc}^{-3}$. Taking an alternative approach, if we consider the distances provided by Gaia DR3 for the low-quality WDs, then 181 WDs are present within 1kpc. Under the assumption that the WDs density is homogeneous and isotropic throughout 1kpc, the space density reaches $\sim 1.3 \times 10^{-3} \text{ pc}^{-3}$, higher than most of the literature estimates given in Verbeek et al. (2013, Table 3). Our upper limit of global (up to 1 kpc) WD space density agrees with the local (< 20 pc) WD space density ($\sim 4 \times 10^{-3} \text{ pc}^{-3}$) estimated using Gaia EDR3 by Gentile Fusillo et al. (2021). This showcases the need for deep UV photometry to identify Galactic WDs. However, it is well known throughout the literature that the WD population model changes with thin disc, thick disc and the halo (Bianchi et al. 2011). Hence, it is clear that UV photometry, in combination with Gaia future releases, can be used to better estimate the space density of WDs, given the structure of the Galaxy. Large-scale WD detection studies combining UV and Gaia are necessary to accurately estimate the WD density in the Galaxy. Future Gaia data releases will constrain the astrometry of these low-quality WDs better.

5. Summary

In this study, we have demonstrated the capabilities of UVIT to identify and characterise the WDs in the Galaxy. We made use of the UVIT point source catalogue published by Devaraj et al. (2023) observed towards the outskirts of the SMC region. Further, we crossmatched the UVIT photometry with Gaia DR3 and found that the 273 UV sources with good quality Gaia astrometry and photometry values belong to the Milky Way galaxy rather than to the SMC region. Using colour cuts and SED analysis, we identified 43 single WDs (given in Table 1) in a region in which only 6 WDs were previously detected as WD candidates based on the Gaia DR3 analysis (Gentile Fusillo et al. 2021; Jackim et al. 2024). In addition to 43 WDs, we report the identification of 13 WD+MS candidates (Table 2) and 161 UV bright MS stars (Table B.1).

To estimate the physical characteristics of the identified WDs in our sample, we follow a common method adopted in literature (Nayak et al. 2024; Karinkuzhi et al. 2024) using the ‘WD_models’ open-source python package. The package estimates the mass and age of the WDs by finding the closest atmosphere grid and cooling model based on the position in the Gaia CMD. We find that the masses of WDs identified in this

study range from $0.2 M_{\odot}$ to $1.3 M_{\odot}$ and the T_{eff} from 10000 K to 15000 K. Cooling ages of these WDs range from 0.1 Gyr to 2 Gyr. In comparison to the bonafide sample of WDs (MWDD), we find that our sample of WDs has higher temperatures owing to the detection through UVIT. We note that the estimated mass and the cooling age of WDs identified in this work match well with the literature values from MWDD. Furthermore, we report the detection of 20 ELM candidates based on their position in the Gaia CMD and SED analysis. Further detailed studies and spectroscopic confirmation of these sources will lead to a better understanding of their formation processes. Given the limitations of Gaia DR3 distance measurements of optically faint WDs, we discuss the completeness and estimates of the WD space density through our sample. Back-of-the-envelope calculations show that the estimated WD space density within 1kpc can be two orders of magnitude larger than previous estimates.

Our results not only highlight the instrumental effectiveness of UVIT but also anticipate the potential of upcoming dedicated UV missions like INSIST. These missions are premier instruments for the systematic discovery of WDs and other diverse stellar systems, providing invaluable insights into the complex dynamics of binary systems within our galaxy. As we conclude this study within the current FoV, our analytical approach will be extended to unveil additional WD systems in other fields observed by UVIT (Piridi et al. 2024; Mondal et al. 2023; Leahy et al. 2020). The subsequent phase involves the critical follow-up step of spectroscopic surveys. This effective blend of follow-up observations and thorough analysis establishes UVIT and upcoming missions as crucial contributors to enhancing our understanding of stellar systems in the ultraviolet domain.

Acknowledgements. We thank the reviewer for their valuable comments and suggestions, which have improved the manuscript. We are grateful to the Centre for Research, CHRIST (Deemed to be University), Bangalore, for the research grant extended to carry out the current project through the SEED money project (SMSS-2335, 11/2023). We thank the SIMBAD database and the online VizieR library service for helping us with the literature survey and obtaining relevant data. This publication uses the data from the UVIT, which is part of the AstroSat mission of the ISRO, archived at the Indian Space Science Data Centre (ISSDC). This work has made use of data from the European Space Agency (ESA) mission Gaia (<https://www.cosmos.esa.int/Gaia>), processed by the Gaia Data Processing and Analysis Consortium (DPAC, <https://www.cosmos.esa.int/web/Gaia/dpac/consortium>). Funding for the DPAC has been provided by national institutions, in particular, the institutions participating in the Gaia Multilateral Agreement. This publication makes use of VOSA, developed under the Spanish Virtual Observatory (<https://svo.cab.inta-csic.es>) project funded by MCIN/AEI/10.13039/501100011033/ through grant PID2020-112949GB-I00. VOSA has been partially updated by using funding from the European Union's Horizon 2020 Research and Innovation Programme, under Grant Agreement n° 776403 (EXOPLANETS-A).

References

Allard, F., Homeier, D., & Freytag, B. 2011, in *Astronomical Society of the Pacific Conference Series*, Vol. 448, 16th Cambridge Workshop on Cool Stars, Stellar Systems, and the Sun, ed. C. Johns-Krull, M. K. Browning, & A. A. West, 91

Allard, F., Homeier, D., & Freytag, B. 2012, *Philosophical Transactions of the Royal Society of London Series A*, 370, 2765

Arun, R., Mathew, B., Maheswar, G., et al. 2021, *Monthly Notices of the Royal Astronomical Society*, 507, 267

Bailer-Jones, C., Rybizki, J., Fousneau, M., Demleitner, M., & Andrae, R. 2021, *The Astronomical Journal*, 161, 147

Baraffe, I., Homeier, D., Allard, F., & Chabrier, G. 2015, *Astronomy & Astrophysics*, 577, A42

Bayo, A., Rodrigo, C., y Navascués, D. B., et al. 2008, *Astronomy & Astrophysics*, 492, 277

Bédard, A., Bergeron, P., Brassard, P., & Fontaine, G. 2020, *The Astrophysical Journal*, 901, 93

Bédard, A., Bergeron, P., & Fontaine, G. 2017, *The Astrophysical Journal*, 848, 11

Bhattacharyya, S., Mathew, B., Ezhikode, S. H., et al. 2022, *The Astrophysical Journal Letters*, 933, L34

Bianchi, L. 2009, *Astrophysics and Space Science*, 320, 11

Bianchi, L., Efremova, B., Herald, J., et al. 2011, *Monthly Notices of the Royal Astronomical Society*, 411, 2770

Boyer, M. L., Srinivasan, S., van Loon, J. T., et al. 2011, *The Astronomical Journal*, 142, 103

Brown, A. G., Vallenari, A., Prusti, T., et al. 2021, *Astronomy & Astrophysics*, 649, A1

Brown, A. G., Vallenari, A., Prusti, T., et al. 2016, *Astronomy & Astrophysics*, 595, A2

Brown, W. R., Kilic, M., Kosakowski, A., & Gianninas, A. 2022, *The Astrophysical Journal*, 933, 94

Cheng, S., Cummings, J. D., Ménard, B., & Toonen, S. 2020, *The Astrophysical Journal*, 891, 160

Choi, J., Dotter, A., Conroy, C., et al. 2016, *The Astrophysical Journal*, 823, 102

Cruzalèbes, P., Petrov, R., Robbe-Dubois, S., et al. 2019, *Monthly Notices of the Royal Astronomical Society*, 490, 3158

Dattatreya, A. K., Yadav, R., Kumawat, G., et al. 2023a, *Monthly Notices of the Royal Astronomical Society: Letters*, 523, L58

Dattatreya, A. K., Yadav, R., Rani, S., et al. 2023b, *The Astrophysical Journal*, 943, 130

De Grijs, R. & Bono, G. 2015, *The Astronomical Journal*, 149, 179

Devaraj, A., Joseph, P., Stalin, C., Tandon, S. N., & Ghosh, S. K. 2023, *The Astrophysical Journal*, 946, 65

Dotter, A. 2016, *The Astrophysical Journal Supplement Series*, 222, 8

Dufour, P., Blouin, S., Coutu, S., et al. 2016, arXiv preprint arXiv:1610.00986

Eisenstein, D. J., Liebert, J., Harris, H. C., et al. 2006, *The Astrophysical Journal Supplement Series*, 167, 40

Florsch, A. 1972, *Publication de l'Observatoire de Strasbourg*, 2, 1

Fontaine, G., Brassard, P., & Bergeron, P. 2001, *Publications of the Astronomical Society of the Pacific*, 113, 409

Gaia, C., Brown, A., Vallenari, A., et al. 2018, *Astronomy & Astrophysics*, 616

Gaia Collaboration, Vallenari, A., Brown, A. G., Prusti, T., et al. 2023, *Astronomy & Astrophysics*, 674, A1

Gentile Fusillo, N., Tremblay, P.-E., Cukanovaite, E., et al. 2021, *Monthly Notices of the Royal Astronomical Society*, 508, 3877

Gentile Fusillo, N. P., Tremblay, P.-E., Gänsicke, B. T., et al. 2019, *Monthly Notices of the Royal Astronomical Society*, 482, 4570

Gómez de Castro, A. I. & Barstow, M. A. 2007, *UV Astronomy: Stars from Birth to Death*

Groot, P. J., Verbeek, K., Greimel, R., et al. 2009, *Monthly Notices of the Royal Astronomical Society*, 399, 323

Hutchings, J. 1982, *The Astrophysical Journal*, 255, 70

Istrate, A., Tauris, T., & Langer, N. 2014a, *Astronomy & Astrophysics*, 571, A45

Istrate, A., Tauris, T., Langer, N., & Antoniadis, J. 2014b, *Astronomy & Astrophysics*, 571, L3

Jackim, R., Heyl, J., & Richer, H. 2024, arXiv preprint arXiv:2404.07388

Jadhav, V. V., Sindhu, N., & Subramaniam, A. 2019, *The Astrophysical Journal*, 886, 13

Jiménez-Esteban, F., Torres, S., Rebassa-Mansergas, A., et al. 2018, *Monthly Notices of the Royal Astronomical Society*, 480, 4505

Karinkuzhi, D., Mukhopadhyay, B., Wickramasinghe, D., & Tout, C. A. 2024, *Monthly Notices of the Royal Astronomical Society*, stae829

Kepler, S. O., Koester, D., Pelisoli, I., Romero, A. D., & Ourique, G. 2021, *Monthly Notices of the Royal Astronomical Society*, 507, 4646

Kepler, S. O., Pelisoli, I., Koester, D., et al. 2016, *Monthly Notices of the Royal Astronomical Society*, 455, 3413

Kepler, S. O., Pelisoli, I., Koester, D., et al. 2019, *Monthly Notices of the Royal Astronomical Society*, 486, 2169

Khurana, A., Chawla, C., & Chatterjee, S. 2023, *The Astrophysical Journal*, 949, 102

Kilic, M., Stanek, K., & Pinsonneault, M. 2007, *The Astrophysical Journal*, 671, 761

Koester, D. 2010, *Memorie della Societa Astronomica Italiana*, 81, 921

Kumar, A., Ghosh, S., Hutchings, J., et al. 2012, in *Space Telescopes and Instrumentation 2012: Ultraviolet to Gamma Ray*, Vol. 8443, SPIE, 455–466

Leahy, D. A., Postma, J., Chen, Y., & Buick, M. 2020, *ApJS*, 247, 47

Li, Z., Chen, X., Chen, H.-L., & Han, Z. 2019, *The Astrophysical Journal*, 871, 148

Mondal, C., Saha, K., Bhattacharya, S., et al. 2023, *ApJS*, 264, 40

Morrissey, P., Conrow, T., Barlow, T. A., et al. 2007, *The Astrophysical Journal Supplement Series*, 173, 682

Nandez, J. L., Ivanova, N., & Lombardi Jr, J. C. 2015, *Monthly Notices of the Royal Astronomical Society: Letters*, 450, L39

Nayak, P. K., Ganguly, A., & Chatterjee, S. 2024, *Monthly Notices of the Royal Astronomical Society*, 527, 6100

Panthi, A., Subramaniam, A., Vaidya, K., et al. 2023, *Monthly Notices of the Royal Astronomical Society*, 525, 1311

- Panthi, A. & Vaidya, K. 2024, *Monthly Notices of the Royal Astronomical Society*, 527, 10335
- Parsons, S., Gänsicke, B. T., Marsh, T., et al. 2017, *Monthly Notices of the Royal Astronomical Society*, 470, 4473
- Parsons, S., Rebassa-Mansergas, A., Schreiber, M. R., et al. 2016, *Monthly Notices of the Royal Astronomical Society*, 463, 2125
- Pecaut, M. J. & Mamajek, E. E. 2013, *The Astrophysical Journal Supplement Series*, 208, 9
- Pelisolì, I. & Vos, J. 2019, *Monthly Notices of the Royal Astronomical Society*, 488, 2892
- Piridi, S., Kumar, R., Pandey, D., & Pradhan, A. C. 2024, in 42nd meeting of the Astronomical Society of India (ASI), O46
- Prabhu, D. S., Subramaniam, A., Sahu, S., et al. 2022, *The Astrophysical Journal Letters*, 939, L20
- Rebassa-Mansergas, A., Ren, J., Irawati, P., et al. 2017, *Monthly Notices of the Royal Astronomical Society*, 472, 4193
- Rebassa-Mansergas, A., Solano, E., Jiménez-Esteban, F. M., et al. 2021, *Monthly Notices of the Royal Astronomical Society*, 506, 5201
- Ren, J.-J., Raddi, R., Rebassa-Mansergas, A., et al. 2020, *The Astrophysical Journal*, 905, 38
- Sahu, S., Subramaniam, A., Singh, G., et al. 2022, *Monthly Notices of the Royal Astronomical Society*, 514, 1122
- Sharpee, B., Stark, M., Pritzl, B., et al. 2002, *The Astronomical Journal*, 123, 3216
- Shridharan, B., Mathew, B., Bhattacharyya, S., et al. 2022, *Astronomy & Astrophysics*, 668, A156
- Sindhu, N., Subramaniam, A., Jadhav, V. V., et al. 2019, *The Astrophysical Journal*, 882, 43
- Soszynski, I., Udalski, A., Szymanski, M., et al. 2016, arXiv preprint arXiv:1601.01318
- Stecher, T. P., Cornett, R. H., Greason, M. R., et al. 1997, *Publications of the Astronomical Society of the Pacific*, 109, 584
- Steinmetz, M., Guiglion, G., McMillan, P. J., et al. 2020, *The Astronomical Journal*, 160, 83
- Subramaniam, A. et al. 2018, *Monthly Notices of the Royal Astronomical Society*, 481, 226
- Tandon, S., Hutchings, J., Ghosh, S., et al. 2017a, *Journal of Astrophysics and Astronomy*, 38, 1
- Tandon, S., Postma, J., Joseph, P., et al. 2020, *The Astronomical Journal*, 159, 158
- Tandon, S., Subramaniam, A., Girish, V., et al. 2017b, *The Astronomical Journal*, 154, 128
- Vaidya, K., Panthi, A., Agarwal, M., et al. 2022, *Monthly Notices of the Royal Astronomical Society*, 511, 2274
- Verbeek, K., Groot, P. J., Nelemans, G., et al. 2013, *Monthly Notices of the Royal Astronomical Society*, 434, 2727
- York, D. G., Adelman, J., Anderson Jr, J. E., et al. 2000, *The Astronomical Journal*, 120, 1579
- Zacharias, N., Finch, C., Girard, T., et al. 2013, *The astronomical journal*, 145, 44

**Appendix A: Crossmatch of 273 sources with
SIMBAD**

**Appendix B: The list of MS sources identified in
this study**

Table A.1. List of 35 sources from the 273 sources which had a literature match.

RA (deg)	DEC (deg)	ID	Object Type	Reference
17.324315622255	-71.5451385177136	Flo 562	Star	Brown et al. (2021)
17.7106502826721	-71.2916943448284	SSTISAGEMA J011050.63-711730.0	Star	Boyer et al. (2011)
16.6796158981582	-71.2218013983896	OGLE SMC-CEP-4797	deltaCep	Soszynski et al. (2016)
17.1564487311332	-71.3318689685798	Gaia DR3 4690615216552295808	WD*_Candidate	Gentile Fusillo et al. (2021)
16.7713529712995	-71.4256416321197	Flo 520	Star	Florsch (1972)
17.5136828428392	-71.3366073814231	Gaia DR2 4690569105783446016	Star	Pelisolì & Vos (2019)
17.3156836844279	-71.3590784755199	Gaia DR3 4690615560150914560	WD*_Candidate	Gentile Fusillo et al. (2021)
17.0009874928717	-71.2656175718428	SSTISAGEMA J010800.18-711556.2	RGB*_Candidate	Boyer et al. (2011)
17.4063434253079	-71.2274672874512	SSTISAGEMA J010937.59-711338.8	RGB*_Candidate	Boyer et al. (2011)
17.0007632587125	-71.250989567725	Gaia DR2 4690619477160130944	WD*_Candidate	Jiménez-Esteban et al. (2018); Gentile Fusillo et al. (2021)
17.3720747932814	-71.3629982597683	SSTISAGEMA J010929.22-712146.6	Star	Boyer et al. (2011)
17.9879044542788	-71.326669251763	Gaia DR3 4690659300093357184	WD*_Candidate	Gentile Fusillo et al. (2021)
17.2080457654542	-71.4322737820098	SSTISAGEMA J010849.92-712556.5	Star	Boyer et al. (2011)
17.7072269440675	-71.2462944249463	Gaia DR3 4690710225517000064	WD*_Candidate	Gentile Fusillo et al. (2021); Jackim et al. (2024)
17.200465789012	-71.2471671891088	V* AI Tuc	RRLyr	Soszynski et al. (2016)
16.7111946726546	-71.3198202304278	Gaia DR3 4690613017528995840	WD*_Candidate	Gentile Fusillo et al. (2021)
17.5947497588541	-71.2204588186018	Flo 580	Star	Cruzalèbes et al. (2019)
16.6573235791628	-71.3043469573808	HD 6782	PM*	Brown et al. (2016)
17.2261501076935	-71.1290625783677	CD-71 52	Star	Cruzalèbes et al. (2019)
16.7975558874761	-71.4394252973841	AzV 107F	Star	Zacharias et al. (2013)
16.9785321749041	-71.3302517486784	TYC 9139-2292-1	Star	Steinmetz et al. (2020)
16.5374945763772	-71.2857297762281	[SSP2002] E	Star	Sharpee et al. (2002)
16.6198321911708	-71.2204758069251	SSTISAGEMA J010628.75-711313.9	Star	Boyer et al. (2011)
16.5784454988714	-71.1965697551032	Flo 511	Star	Steinmetz et al. (2020)
17.3143667205009	-71.4889395826173	Gaia DR3 4690562719174050048	WD*_Candidate	Jackim et al. (2024)
17.399210952441	-71.305061697809	Gaia DR3 4690616011131760384	WD*_Candidate	Jackim et al. (2024)
17.1521486208823	-71.3926117140705	Gaia DR3 4690613949547518208	WD*_Candidate	Jackim et al. (2024)
17.1569075977901	-71.2475319062813	Gaia DR3 4690618759910796544	WD*_Candidate	Jackim et al. (2024)
17.1815225128217	-71.3598163557577	Gaia DR3 4690614327504623360	WD*_Candidate	Jackim et al. (2024)
17.2538839850791	-71.3606027456645	Gaia DR3 4690614155705930112	WD*_Candidate	Jackim et al. (2024)
17.8060768911678	-71.4725313365736	Gaia DR3 4690551758417486336	WD*_Candidate	Jackim et al. (2024)
16.8059214822535	-71.2131825819021	Gaia DR3 4690631335569472512	WD*_Candidate	Jackim et al. (2024)
17.2789677473114	-71.1703183236006	Gaia DR3 4690621508690057216	WD*_Candidate	Jackim et al. (2024)
17.2469723278347	-71.315952637468	Gaia DR3 4690616659661394304	WD*_Candidate	Jackim et al. (2024)
17.3713081454728	-71.2185421124811	Gaia DR3 4690620203019782400	WD*_Candidate	Jackim et al. (2024)

Table B.1. List of the 161 MS stars identified from the present study

Gaia DR3 ID	RA (deg)	DE (deg)	Distance (pc)	N263M (mag)		N245M (mag)		N279N (mag)		F172M (mag)		F169M (mag)		F154W (mag)		N219M (mag)		T_{eff} (K)	$logg$
				AB	Error														
4.69062518518192E+018	16.57654	-71.29023	507.751678	20.297	0.064	21.432	0.095	19.7	0.09									5400	5
4.690561516583326E+018	17.32432	-71.54514	801.134888	19.262	0.04	20.908	0.075	18.391	0.05									4600	4.5
4.69066191142658E+018	17.86988	-71.32645	2866.5105	20.41	0.049	21.052	0.058	20.18	0.081									6500	3.5
4.6907112219494E+018	17.59475	-71.22046	643.002869	14.677	0.003	15.562	0.004	14.54	0.005	18.268	0.023	19.282	0.028	19.61	0.033	15.712	0.013	6600	5
4.69062542570005E+018	16.73223	-71.24065	874.526184	21.832	0.13			21.208	0.181									5400	4
4.69056725465948E+018	17.36359	-71.44183	1165.23694	19.1	0.021	20.186	0.031	19.185	0.042							20.677	0.097	6100	4
4.69061721372258E+018	17.44166	-71.27038	1316.94849	19.371	0.025	20.555	0.038	18.96	0.037									5900	4.5
4.69066205316384E+018	17.77782	-71.32738	2212.08789	19.087	0.027	19.847	0.033	19.058	0.049							19.908	0.067	6800	4
4.69056811365289E+018	17.58723	-71.35238	6141.80762	21.393	0.079	21.762	0.111	21	0.163									7600	5
4.69054941767336E+018	17.35431	-71.5906	1954.15002	20.919	0.087													6200	5
4.69062178356771E+018	17.48629	-71.13251	2494.0332	20.166	0.061	21.452	0.096	19.742	0.091									6100	5
4.69056694111955E+018	17.21182	-71.41501	277.851501	21.561	0.117	21.623	0.075	21.22	0.181	22.647	0.288							10800	0
4.69056621956637E+018	17.09981	-71.4748	4935.03955	20.619	0.046	20.992	0.046	20.419	0.075									7400	5
4.69056079502881E+018	17.21656	-71.5914	579.67865									22.023	0.184					6000	4
4.69061195668268E+018	16.82167	-71.35748	804.726807	17.588	0.013	18.738	0.02	17.34	0.022							19.27	0.066	5900	4
4.69061553009542E+018	17.19522	-71.29023	2148.69604	21.492	0.085			20.997	0.163									6200	5
4.69062494466375E+018	16.66549	-71.29562	1007.41357	18.421	0.027	19.564	0.04	18.335	0.048									6200	5
4.69062494466376E+018	16.65732	-71.30435	98.0849609	14.948	0.005	14.361	0.005	13.126	0.005			18.679	0.036	19.115	0.045	15	0.009	6000	4
4.6906144649436E+018	16.89218	-71.40272	1923.59192	19.756	0.029	21.188	0.05	19.706	0.053									5800	4
4.69063133557504E+018	16.77777	-71.22784	5439.14746	19.785	0.051	20.799	0.071	19.576	0.085									5900	5
4.69071101149303E+018	17.82407	-71.1799	2426.38867	20.819	0.083	21.787	0.112	20.582	0.135									6100	4
4.69061717936283E+018	17.34527	-71.24876	2390.42529	19.987	0.033	21.234	0.053	19.843	0.056									6100	4
4.69071015679753E+018	17.70098	-71.2569	594.829712	19.153	0.022	20.514	0.036	18.713	0.033									5500	4.5
4.69055144917987E+018	17.7799	-71.50898	764.347961	17.901	0.022	19.022	0.031	17.65	0.036							19.331	0.076	6100	5
4.69064449533761E+018	17.88163	-71.51531	1103.61462	19.682	0.049	21.184	0.085	19.374	0.079									5800	4.5
4.69061951582505E+018	17.0205	-71.24934	1337.36548	17.618	0.013	18.464	0.017	17.466	0.023	21.768	0.144	21.95	0.178	22.245	0.191	18.612	0.035	6600	5
4.6905509681436E+018	17.49441	-71.5691	1432.04077	20.309	0.066			19.894	0.101									5900	5
4.69062043923299E+018	17.29293	-71.1	1625.68982	20.146	0.043	21.416	0.071	19.937	0.073									6200	4.5
4.69061298747482E+018	16.75535	-71.32757	1448.65942	21.356	0.105													5600	4
4.6906198594224E+018	17.13099	-71.20618	2383.63672	19.409	0.03	20.315	0.041	19.249	0.052							20.639	0.091	6400	5
4.69065947618345E+018	18.01465	-71.29682	1934.09143	20.485	0.071			20.013	0.104									5800	4
4.69056220377801E+018	17.18624	-71.52321	2001.50391	20.222	0.063	21.349	0.092	20.169	0.114									6100	3.5
4.69056584591023E+018	17.25588	-71.46314	392.160675	19.036	0.021	20.413	0.035	18.464	0.03									5300	4.5
4.6906165222265E+018	17.55176	-71.26899	3659.71973	20.987	0.052			20.902	0.113									6600	4.5
4.6907148297219E+018	17.61696	-71.13598	3342.55542	20.816	0.083			20.594	0.135									6300	4
4.69062119945219E+018	17.28052	-71.1939	8176.15332	20.519	0.052	21.951	0.121	20.186	0.081									5400	5
4.69065782691309E+018	17.87784	-71.40297	1653.60144	18.981	0.025	19.933	0.034	18.911	0.045							20.16	0.111	6400	4.5
4.69056670490367E+018	17.16157	-71.43209	208.265167	21.065	0.054			19.962	0.062									4600	5.5
4.69063356895797E+018	17.18656	-71.12657	2213.52783	19.39	0.042	20.407	0.059	19.238	0.073									6400	4
4.69056732337895E+018	17.46448	-71.43648	165.811844					21.177	0.113									3900	6
4.69055117430198E+018	17.58524	-71.52973	508.489746	21.257	0.101			20.537	0.136									5000	5.5
4.69056467767907E+018	17.74985	-71.40001	643.350525	20.903	0.061			20.098	0.078									5200	4
4.69061968762373E+018	17.00041	-71.2434	1048.64355	21.527	0.082			20.904	0.12									5400	5
4.69056213505854E+018	17.1882	-71.53268	3556.75244	20.643	0.076	21.403	0.094	20.525	0.135									6500	4
4.69062016866005E+018	17.31147	-71.22773	3898.67773	21.548	0.116													5600	5
4.69061487726044E+018	16.98475	-71.35109	1013.1073	18.733	0.018	20.072	0.03	18.631	0.032							20.661	0.081	5800	4
4.69061916792237E+018	16.86111	-71.27514	2806.41772	21.509	0.083			21.154	0.175									7000	3
4.69061965326398E+018	17.10539	-71.22253	1057.13074	19.754	0.036	21.153	0.065	19.781	0.074									5900	3.5

Note: This table is truncated to the first 50 entries. The entire contents of this table are available in the electronic version of the article.